JACS
JOURNAL OF THE AMERICAN CHEMICAL SOCIETY

Article

Integrating Metal-Catalyzed C–H and C–O Functionalization to Achieve Sterically Controlled Regioselectivity in Arene Acylation

Nicholas A. Serratore, Constance B. Anderson, Grant B. Frost, Truong-Giang Hoang, Steven Underwood, Philipp Gemmel, Melissa A. Hardy, and Christopher J. Douglas

J. Am. Chem. Soc., **Just Accepted Manuscript** • DOI: 10.1021/jacs.8b06476 • Publication Date (Web): 10 Jul 2018

ACS Publications

is published by the American Chemical Society. 1155 Sixteenth Street N.W., Washington, DC 20036

Integrating Metal-Catalyzed C–H and C–O Functionalization to Achieve Sterically Controlled Regioselectivity in Arene Acylation

Nicholas A. Serratore, Constance B. Anderson, Grant B. Frost[‡], Truong-Giang Hoang[†‡], Steven J. Underwood[‡], Philipp M. Gemmel[⊥], Melissa A. Hardy[§], Christopher J. Douglas*

Department of Chemistry, University of Minnesota – Twin Cities, 207 Pleasant Street SE, Minneapolis, Minnesota 55455

ABSTRACT: One major goal of organometallic chemists is the direct functionalization of the bonds most recurrent in organic molecules: C–H, C–C, C–O, and C–N. An even grander challenge is C–C bond formation when both precursors are of this category. Parallel to this is the synthetic goal of achieving reaction selectivity that contrasts with conventional methods. Electrophilic aromatic substitution (EAS) via Friedel-Crafts acylation is the most renowned method for the synthesis of aryl ketones, a common structural motif of many pharmaceuticals, agrochemicals, fragrances, dyes, and other commodity chemicals. However, an EAS synthetic strategy is only effective if the desired site for acylation is in accordance with the electronic-controlled regioselectivity of the reaction. Herein we report the steric-controlled regioselective arene acylation with salicylate esters via iridium catalysis to access distinctly substituted benzophenones. Experimental and computational data indicate a unique reaction mechanism that integrates C–O activation and C–H activation with a single iridium catalyst without an exogenous oxidant or base. We disclose an extensive exploration of the synthetic scope of both the arene and the ester components, culminating in the concise synthesis of the potent anti-cancer agent hydroxyphenstatin.

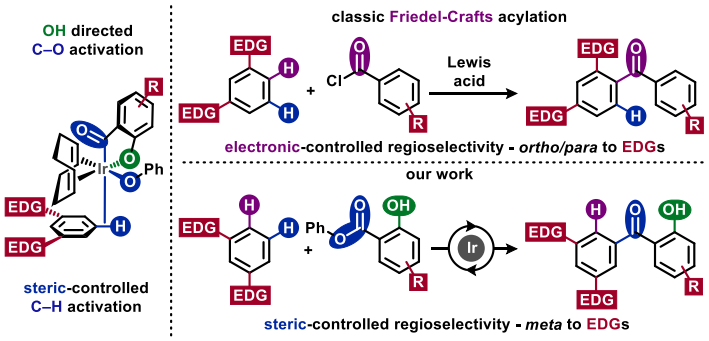

INTRODUCTION

Traditional metal-catalyzed cross-coupling revolutionized both the fields of organometallic catalysis and organic synthesis (**Figure 1, a**).[1] However, the need for metal/halogen pre-functionalization (C–M', C–X) and inevitable production of stoichiometric inorganic waste presented the opportunity for the development of more efficient coupling reactions. To this end, the fields of metal-catalyzed C–H,[2-10] C–C,[11-14] C–N,[15-19] and C–O[20-22] (C–Y) functionalization continue to significantly progress (**Figure 1, b**). Numerous types of reactions involving these groups have been developed, however many still involve one metal/halogen pre-functionalized partner along with stoichiometric exogenous oxidants and/or bases. Combining two metal-catalyzed C–Y activations into a single C–C bond forming reaction is a unique challenge. Recently, the seminal efforts merging C–H with C–H[23] and C–C[24-25] activation have been recognized for their potential to transform synthetic strategy (**Figure 1, c**). There are also a few initial reports of merging C–H with amide C–N[26-27] and anhydride C–O activation.[28-30] However, many of these C–H/C–Y activation reactions still require stoichiometric oxidants and/or bases. The work presented here integrates C–H with ester C_{acyl}–O activation (**Figure 1, d**). Our mechanistic analysis supports both bond

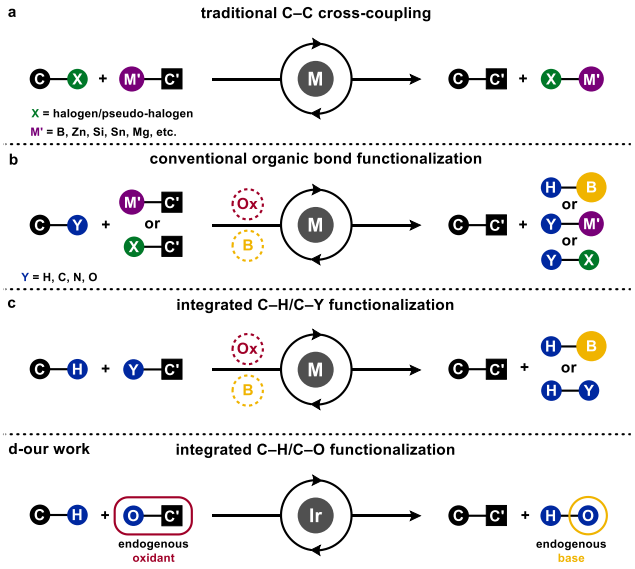

Figure 1. Metal-catalyzed C–C bond forming organic bond functionalization

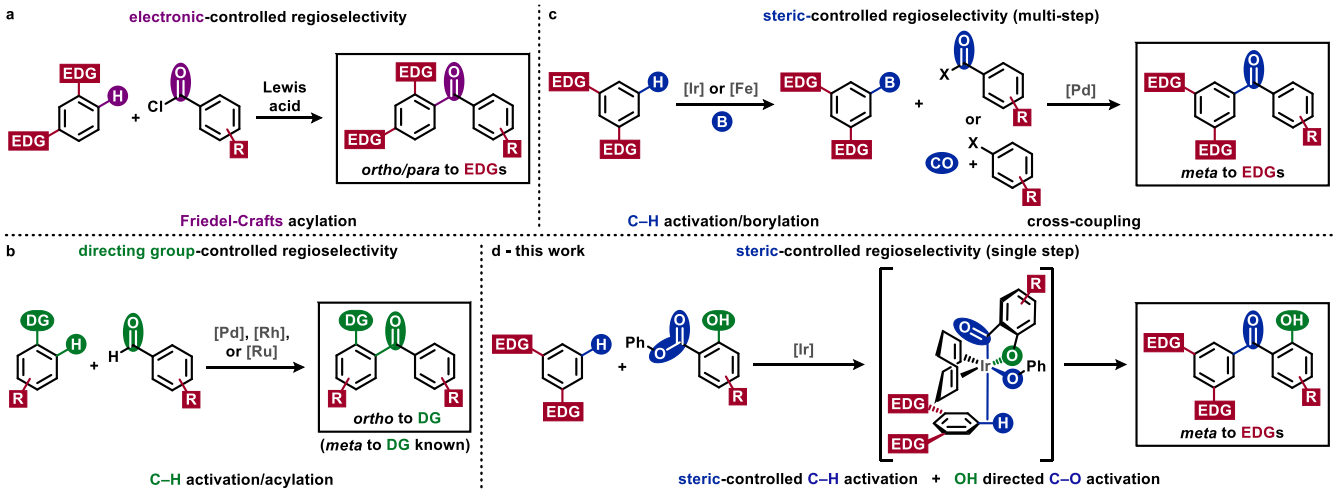

Figure 2. Methods for regioselective acylation. (a) Friedel-Crafts acylation biased by electronics. (b) Directing group-controlled acylation. (c) Potential multi-step steric-controlled acylation, through steric-controlled borylation followed by cross-coupling. (d) Our work: single-step steric-controlled acylation by sequential C_{acyl}–O, C–H bond activation.

activation events occurring at a single iridium catalyst in the catalytic cycle. A conceptual advance in our strategy is using the ester C–O bond to provide an endogenous oxidant as well as a base to complete the catalytic cycle.

Organometallic reaction development also has a rich history of creating new possibilities for synthetic strategy by achieving reaction selectivity counter to the conventions of the time. Modern examples include metal-catalyzed reactions designed to overcome the electronic-controlled regioselectivity of electrophilic aromatic C–H substitutions.[31-38] In Friedel-Crafts reactions electron-donating groups (EDG) direct acylation to the *ortho* and *para* positions, in many cases producing a mixture of products (**Figure 2, a**).[39] Single-site acylation via metal-catalyzed C–H functionalization is typically achieved using a covalently attached or transient directing group (DG, **Figure 2, b**). [28-30,40-41] DG's permit acylation primarily at the *ortho* position (within the regioselectivity purview of Friedel-Crafts acylation) but *meta* selectivity is also known.[42] Steric-controlled regioselective arene acylation is possible, but would require multiple synthetic steps and several precious metal catalysts (**Figure 2, c**). Specifically, iridium[32,35,37-38] or iron-catalyzed[34] C–H borylation may be used to transform the most sterically accessible C–H bond into a C–B bond. Boryl-group manipulation and Suzuki-Miyaura cross coupling would complete the acylation.[43-44] We are unaware of any steric-controlled C–H bond functionalization method for acylation with a single catalyst. Our iridium-catalyzed sequential bond activation of an ester C_{acyl}–O bond and an arene C–H bond permits single-step, steric-controlled, regioselective arene acylation (**Figure 2, d**).

During our investigations into iridium-catalyzed C_{acyl}–O bond activation of salicylate esters for intramolecular alkene oxyacylation,[45] we discovered the intermolecular acylation of the solvent, *m*-xylene (**Scheme 1**). The major regioisomer of this acylation was the sterically-favored *meta*-substituted product. Control experiments (see supporting information, Table S1) showed that iridium was required for product formation and phosphine improved the yield of

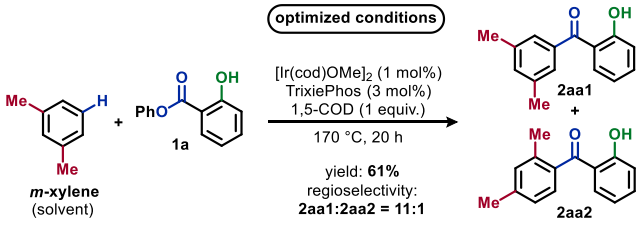

Scheme 1. Optimized reaction conditions.

product. Optimized reaction conditions (see supporting information, Tables S2–S8) for the acylation of the solvent, *m*-xylene, with phenyl salicylate gave the *meta*- and *ortho*/*para*-substituted products (**2aa1** and **2aa2**) in an 11:1 ratio. Further, the 11:1 ratio did not change over time as observed by ^{1}H NMR, suggesting kinetic selectivity. This regioselectivity directly contrasts with classic Friedel-Crafts acylation of *m*-xylene with benzoyl chloride, where the *ortho*-/*para*- and di-*ortho*-substituted products were greatly favored over *meta*-substitution (99:1).[46] This comparison highlights that our new reaction is not dictated by electronic-controlled regioselectivity.

RESULTS

We find the two mechanistic paths shown for our acylation reaction to be most plausible **(Scheme 2)**. These paths are based on our results and analysis that follow. Phenyl salicylate **1** coordinates to $[Ir(cod)OMe]_2$ (**A**): breaking the dimer, liberating methanol, and forming square planar intermediate **I**, the proposed resting-state of the catalyst. Relative to catalyst loading, approximately two equivalents of methyl salicylate **II** were observed, suggesting sacrificial transesterification of **1** with methanol (**B**). Oxidative addition into the C_{acyl}–OPh bond of **I** (**C**) forms square pyramidal complex **III**.[47] This step and all subsequent steps are proposed to be reversible. From **III**, multiple pathways are plausible. First, the limiting factor in catalyst lifetime is pro-

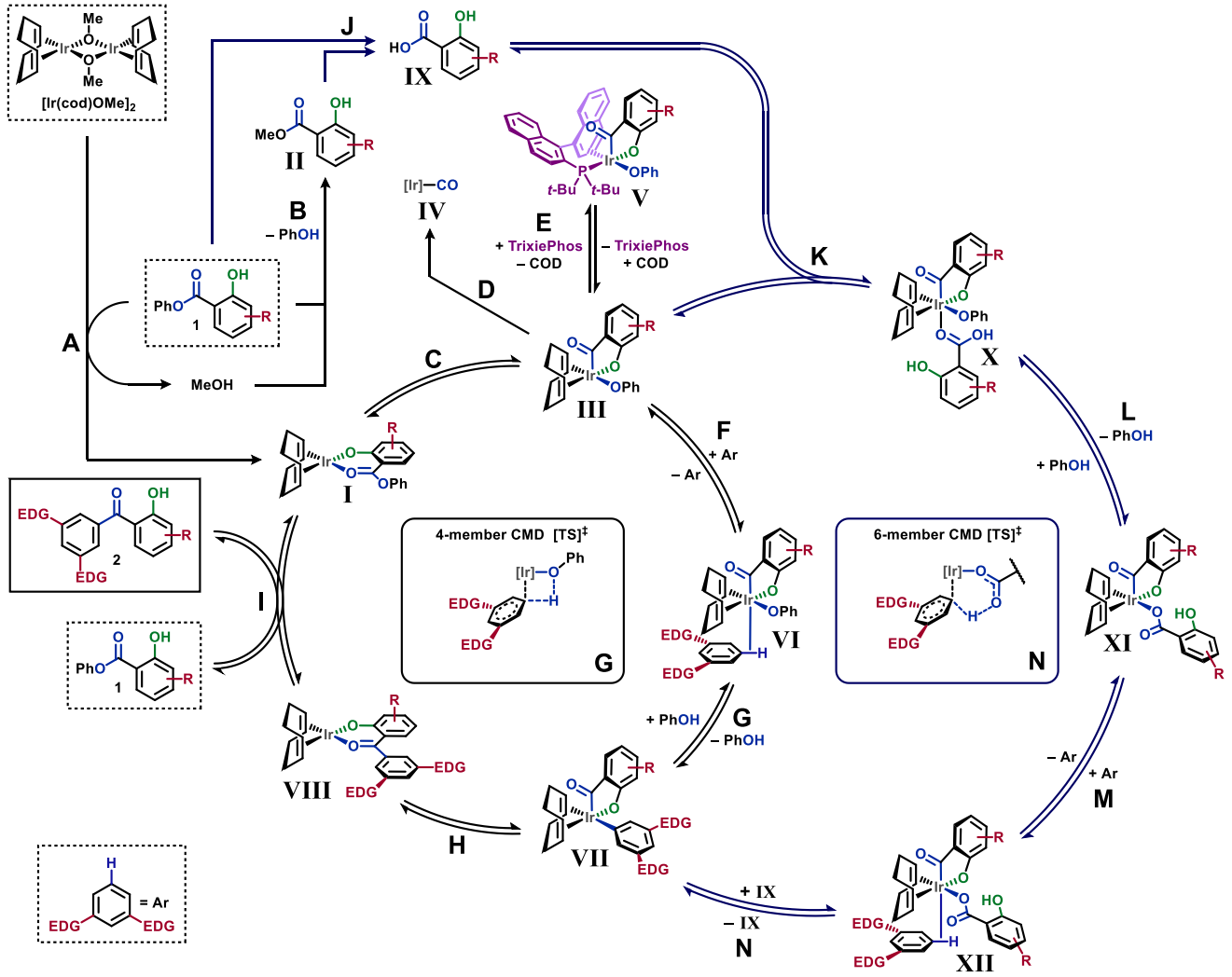

Scheme 2. Plausible mechanisms via either a 4-member or 6-member CMD transition state.

posed to be decarbonylation (**D**) to irreversibly form iridium carbonyl complex **IV**. TrixiePhos is proposed to inhibit this decomposition by reversibly displacing COD (**E**), stabilizing the C_{acyl}–O oxidative addition intermediate off-cycle as **V**.[48] **III** may continue the productive path through coordination of the arene π-bond followed by σ-adduct formation (**F**) with C_{aryl}–H bond forming **VI**. This leads to the key steric-controlled C–H bond activation step, a 1,2-addition via concerted metalation-deprotonation (CMD) across the Ir–OPh bond (**G**). In this step, a lone pair on the phenoxide oxygen deprotonates the C_{aryl}–H through a 4-member transition state, forming phenol and the new Ir–C_{aryl} complex **VII**.[49] Reductive elimination (**H**) forms the new C_{acyl}–C_{aryl} bond, giving square planar **VIII** with new acylation product **2** bound to iridium. Finally, ligand exchange of **2** for **1** (**I**) regenerates intermediate **I**.

An alternative mechanism involving a more favorable carboxylate-assisted 6-member CMD transition state was also considered.[50] We envision that a formal hydrolysis of **1** or **II** (**J**) could form salicylic acid **IX** to serve as the carboxylate. Either the presence of trace H_2O or possibly an alternative oxidative addition of Ir into the Ph–O or Me–O bond and subsequent protonation may account for the formation of **IX**. **IX** may then enter the catalytic cycle by binding to **III** (**K**) to form octahedral complex **X**. Elimination of phenol (**L**) would then form square pyramidal **XI**. Arene coordination (**M**) would produce **XII**, which may proceed through a less strained 6-member CMD transition state to form **VII**. In either proposed mechanism, the base required to deprotonate the arene is endogenous to the system. In addition, no exogenous oxidant is required for catalyst turnover due to the net reduction of the ester to a ketone over the course of the reaction.

We support our proposed mechanism with evidence from a series of experiments and computations designed to probe key mechanistic aspects of the reaction. H/D kinetic isotope effect (KIE) experiments[51] were performed with d_4-1,2-dimethoxybenzene and 4-d_1-1,2-dimethoxybenzene (**Scheme 3**, **a**). These experiments added insight into the details of arene coordination through C–H cleavage (**III** → **VI** → **VII**).[52] The method of initial rates kinetics was used to determine independent rates for *proteo*- and d_4-1,2-dimethoxybenzene. A $KIE_{inital\ rates}$ = 1.8 ± 0.1 was measured. Product ratios

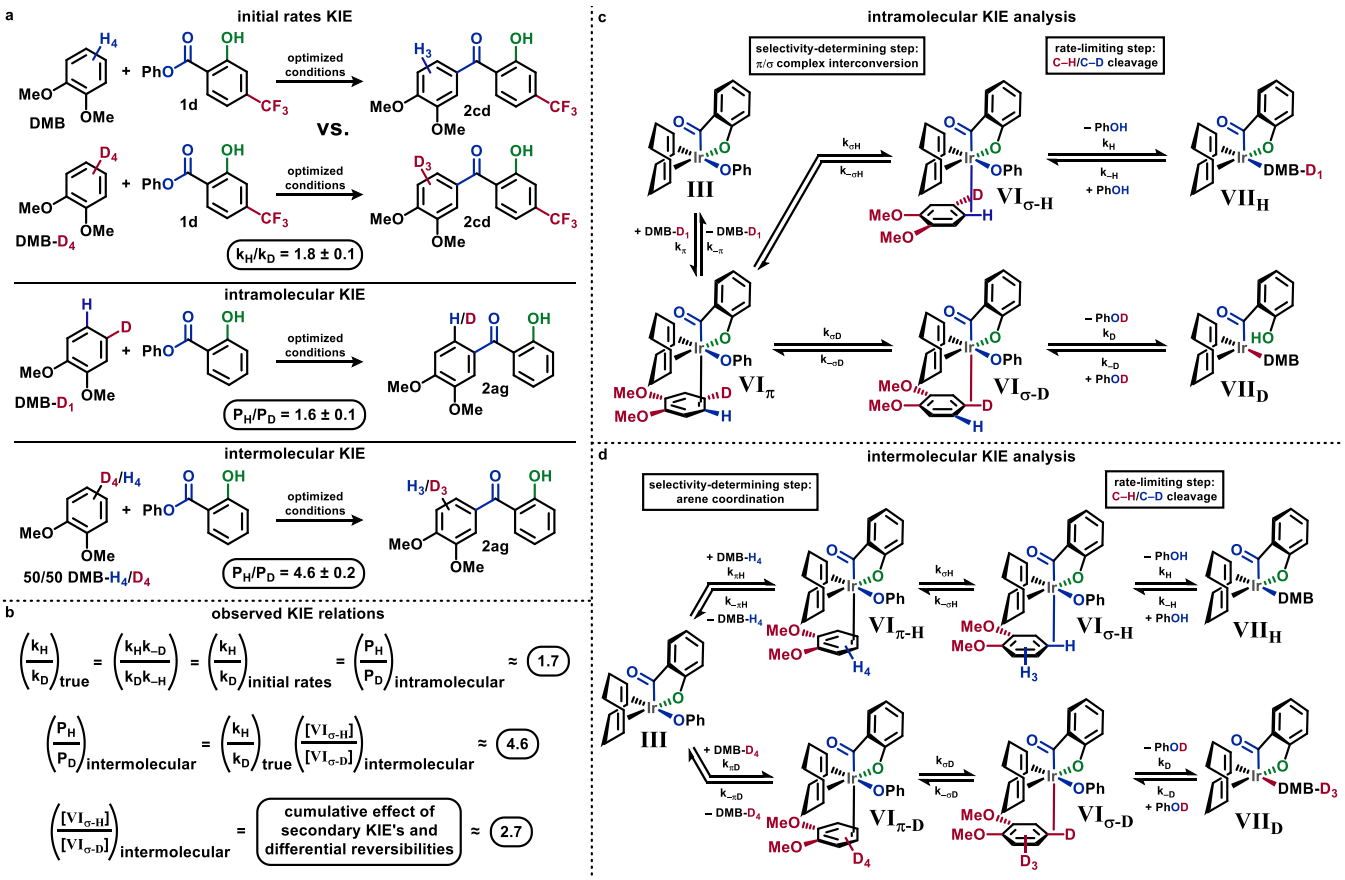

Scheme 3. Mechanistic Analysis (a) Kinetic isotope effect (KIE) experiments. (b) Observed KIE relations and explanation. (c) Intramolecular KIE mechanistic analysis. (d) Intermolecular KIE mechanistic analysis.

were used to determine the KIEs of intramolecular and intermolecular competition experiments. The intramolecular competition with 4-d_1-1,2-dimethoxybenzene gave a similar $KIE_{intramolecular}$ =1.6 ± 0.1, but interestingly the intermolecular competition with a 1:1 mixture of d_4- and *proteo*-1,2-dimethoxybenzene gave an amplified $KIE_{intermolecular}$ = 4.6 ± 0.2.

The observation of separate KIE values for the set of experiments suggests a multistep mechanism from arene coordination to C–H cleavage.[53-54] A primary $KIE_{initial\ rates}$ is evidence that C–H cleavage is the rate-limiting step of the mechanism and a measure of the true KIE of C–H/D cleavage ($(k_H/k_D)_{true}$) (**Scheme 3, b**). Our analysis of the intra- and intermolecular KIE's was primarily influenced by the work of Beak et al.[55] and Adam et al.[56] In the case of the intramolecular KIE we propose that the selectivity bias for H over D abstraction arises from the equilibration of the general arene complex **VI** between σ-adducts (**Scheme 3, c**). $\mathbf{VI_{\sigma\text{-}H}}$ and $\mathbf{VI_{\sigma\text{-}D}}$ may interconvert through $\mathbf{VI_{\pi}}$.[54, 57] This is further evidenced by the fact that $KIE_{intermolecular} \neq KIE_{intramolecular}$ implying that arene coordination is a separate step from the intramolecular selectivity-determining step. If **VI** fully equilibrates between σ-adducts and C–H/D cleavage is rate-limiting ($k_{\sigma H}$, $k_{-\sigma H}$, $k_{\sigma D}$, $k_{-\sigma D}$ >> k_H, k_D) then the observed $KIE_{intramolecular}$ should theoretically reflect ($(k_H/k_D)_{true}$).[55] Our experimental KIE values $KIE_{initial\ rates}$ = 1.8 ± 0.1 and $KIE_{intramolecular}$ =1.6 ± 0.1 are within error and therefore in accordance with this analysis.

In the intermolecular competition reaction, the value of $KIE_{intermolecular}$ = 4.6 ± 0.2 may arise from differential reversibility of arene coordination to **III** (**Scheme 3, d**). This would result in an increased [$\mathbf{VI_{\pi\text{-}H}}$] relative to [$\mathbf{VI_{\pi\text{-}D}}$], which in turn would lead to an increased [$\mathbf{VI_{\sigma\text{-}H}}$] relative to [$\mathbf{VI_{\sigma\text{-}D}}$]. [$\mathbf{VI_{\sigma\text{-}H}}$]/[$\mathbf{VI_{\sigma\text{-}D}}$] is expressed in terms of forward and reverse rate constants (see supporting information), derived with multiple steady-state approximations. The differential reversibility may be explained by secondary isotope effects and/or the preference for H abstraction over D abstraction leading to a higher rate of d_4-1,2-dimethoxybenzene dissociation. This would channel more reacting arene through the proteo-1,2-dimethoxybenzene path.[56] The net effect is measured as an amplification of $(k_H/k_D)_{true}$ by a factor of 2.7. We also note that $KIE_{intermolecular}$ = 4.6 ± 0.2 is comparable to the intermolecular competition KIE found in arene borylation via iridium-catalyzed C–H functionalization (5.0 ± 0.4);[58] and it contrasts with the analogous Friedel-Crafts KIE (1.010 ± 0.0007).[59]

Experiments suggest phosphine is necessary for high turnover of the catalyst, but is not involved in the catalytic cycle. Acylation of 1,2-dimethoxybenzene with **1**, using the optimized reaction conditions, gave >46 turnovers of catalyst versus only 12 turnovers when phosphine was excluded

(see supporting information). Without iridium, no reaction is observed, even with phosphine present. After heating $[Ir(cod)OMe]_2$ with two equivalents of TrixiePhos in 1,2-dimethoxybenzene to 170 °C for one hour, we did not observe a change in the ^{31}P NMR spectra of the reaction mixture. When this same experiment was performed on a reaction mixture containing salicylate **1**, the phosphine signal decreased in intensity over twenty hours. This suggests that phosphine does not bind to the iridium precatalyst. Instead, phosphine may be in a dynamic equilibrium between catalytic intermediate **III** and stable, octahedral complex **V**, potentially slowing the decomposition of catalyst. Phosphine loading studies showed that excess phosphine led to a lower yield of product (see supporting information). This would be expected if phosphine were an inhibitor.

To elucidate the kinetic order of the components of the reaction, rate data was collected for the reaction of phenyl salicylate and 1,2-dimethoxybenzene using the method of initial rates. This data showed zero order with respect to salicylate and 1,5-cyclooctadiene (1,5-COD). The reaction appeared to be greater than first order, however solvent polarity effects could have caused an accelerated reaction at relatively high concentrations of 1,2-dimethoxybenzene. When TrixiePhos was present in concentrations ≥1.8 mM, the reaction was inverse order with respect to phosphine. This region of inverse order is consistent with the off-cycle role of phosphine in our proposed catalytic cycle.

We hypothesize that decarbonylation is the main catalyst decomposition pathway. An infrared spectrum of a crude reaction mixture after twenty hours was taken showing peaks at 1981 and 2027 cm^{-1} (see supporting information), consistent with a catalytically inactive iridium carbonyl complex **IV**.[60] If decarbonylation to form **IV** proceeds via a bimetallic mechanism, we expect that lower concentrations of **III**, induced by phosphine, would slow the rate of decarbonylation (via **VI**) relative to the rate of acylation. Our data are consistent with this hypothesis, suggesting that iridium sequestration by phosphine leads to higher turnover numbers at optimized conditions. In addition, catalyst poisoning under a CO atmosphere inhibits the reaction. An attempted acylation of 1,2-dimethoxybenzene with phenyl salicylate under 1 atm CO results in <10% conversion after 20 hours. We attempted to increase the persistence of our catalyst by acylating 1,2,3-trimethoxybenzene with phenyl salicylate using a reflux apparatus under a flow of N_2, hoping to sweep away CO formed via decarbonylation. We observed similar

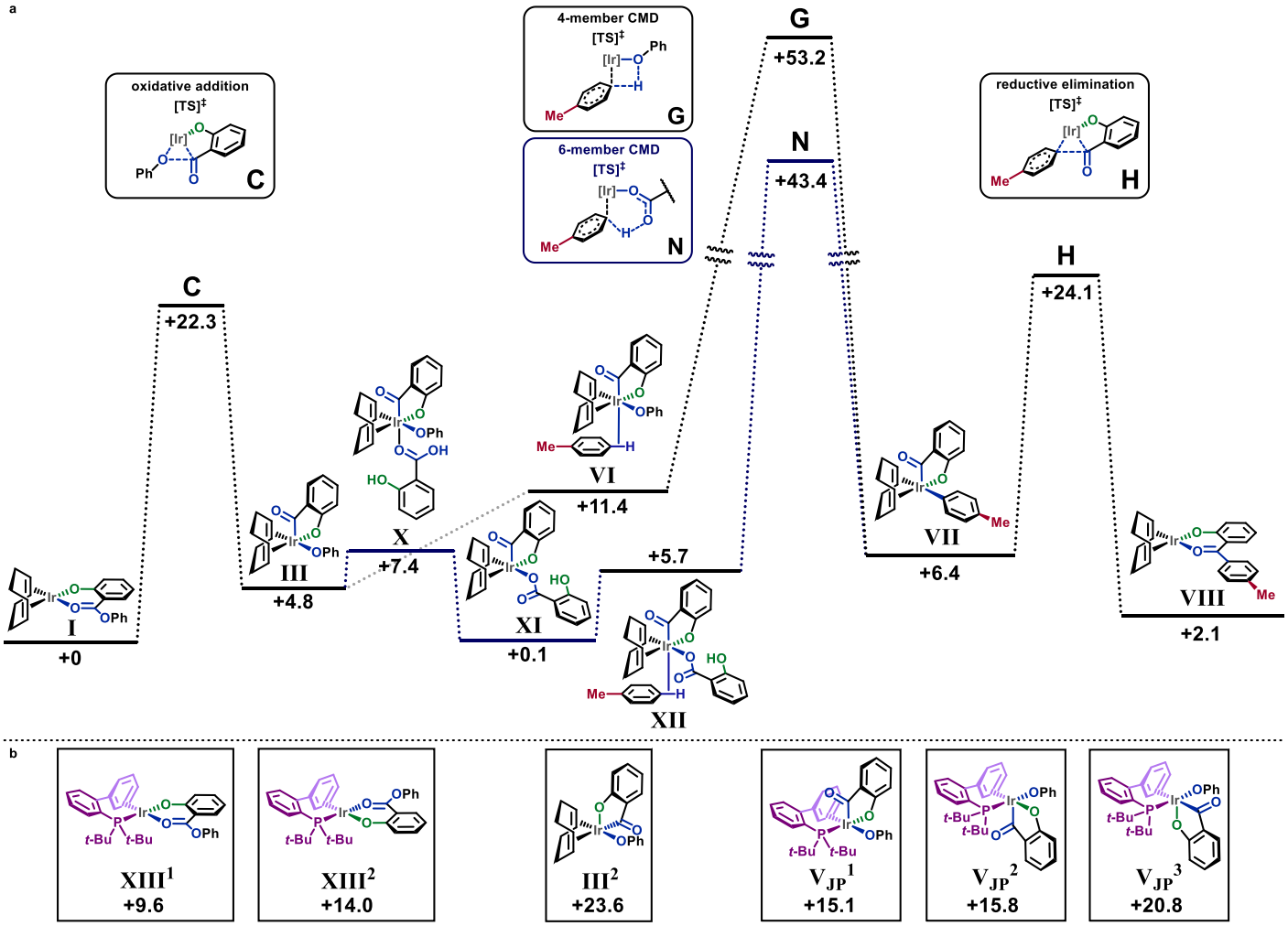

Figure 3. (a) M15-L Computational Analysis. (b) Higher energy configurations and phosphine analogues.

results with this setup as in a sealed vessel. Also, a crucial control experiment to test reversibility of the reaction was performed. The reaction of **2** with excess phenol in mesitylene produced starting ester **1** suggesting the entire cycle is reversible (See supporting information).

A computational investigation into the mechanism of the reaction was pursued using the Gaussian 09 and Gaussian 16 suites (See supporting information for citations). The M06, M06-L, and M15-L density functionals were used to perform these calculations. The 6-31G(d,p) basis sets on H, C, O, and P atoms and the SDD basis set on iridium were used for geometry optimization. The 6-311+G(2df,2pd) basis sets on H, C, O, and P atoms and the SDD basis set on iridium were used for single point energy calculations with SMD solvation using toluene as the solvent. Toluene was therefore chosen as the arene reactant for computational simplicity, although it is likely that the computed barriers would be lower using a more electron-rich arene such as 1,2-dimethoxybenzene. In addition, since JohnPhos performed similarly to TrixiePhos during reaction optimization (see supporting information) we used it as a TrixiePhos analogue to further reduce computational complexity. Overall, the functional that best supported our experimental results was M15-L. This is unsurprising as M15-L was specifically developed to model transition-metal complex thermochemistry.[61] Thus, we chose to only discuss these results in the text.[62]

Comparing **I** to **XIII** and **XIII²**, it is clear that the coordination of phosphine to iridium is uphill relative to COD as an ancillary ligand (**Figure 3, a** and **b**). Inspection of the JohnPhos complexes $\mathbf{V_{JP}^{1-3}}$ shows a large amount of steric congestion around the iridium. This result suggests that COD must fully dissociate if there is an equilibrium between **III** and **V**. The oxidative addition transition state complex **C** has a relative energy of +22.3 kcal which is reasonable given the reaction temperature is 170 °C. The 4-member transition state for CMD **G** is much higher than expected (+53.2 kcal) with the phenoxide deprotonating the arene. Lower transition state energies are known in the literature using carboxylate ligands,[50] which have the advantage of forming more energetically favorable 6-member transition states. A lower energy transition state was sought using a 6-member scaffold. Two possible transition state structures were proposed, a first using a second phenol to coordinate and act as a proton shuttle, forming a 6-member transition state (see supporting information), and a second using the conjugate base of salicylic acid **IX** as a ligand. The transition state with phenol acting as a proton shuttle had a staggeringly high barrier of 67.1 kcal, which suggests this pathway is not accessible in our system. The transition state with salicylate deprotonating the arene **N** has a significantly lower barrier of 43.4 kcal, suggesting that a carboxylate could be acting as our base for CMD. Of particular interest, the reductive elimination product **VIII** is uphill by ~2 kcal, suggesting that the reaction is under thermodynamic equilibrium. Further, the resting state of the catalyst is structure **I**, however **XI** cannot be ruled out based on our computations. The result that the reaction appears to be thermodynamically uphill led us to calculate the theoretical equilibria for a few additional reactions (see supporting information).

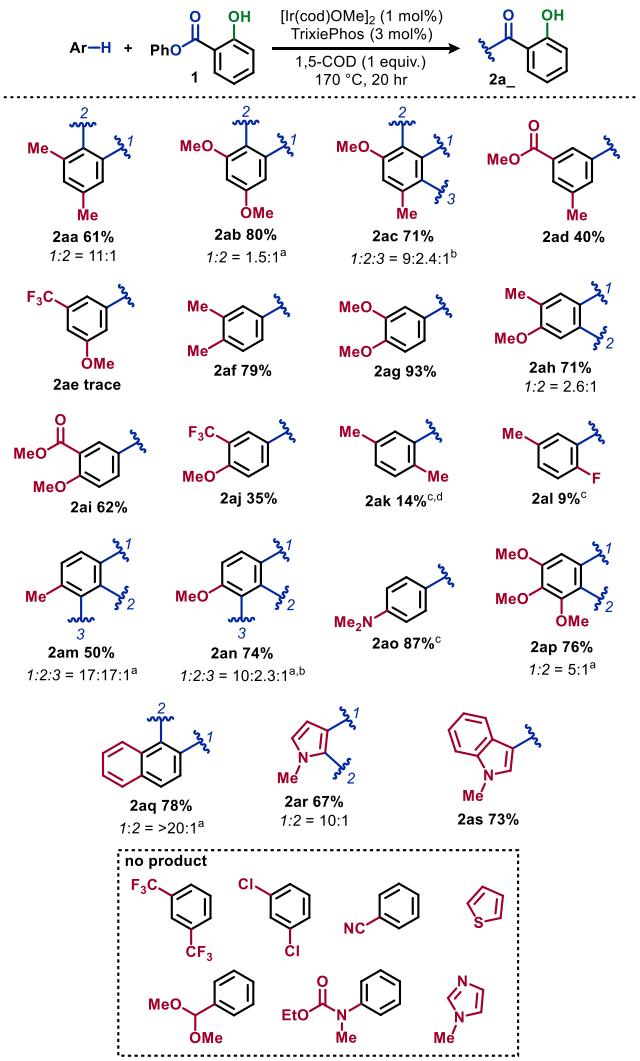

Figure 4. Substrate scope with respect to the arene. Performed with phenyl salicylate **1** (1 equiv), $[Ir(cod)OMe]_2$ (1 mol%), TrixiePhos (3 mol%), 1,5-cyclooctadiene (1,5-COD, 1 equiv), in arene (0.1 M). [a]isolated as an inseparable mixture; product distribution determined by ^{1}H NMR. [b]Minor product **2a_3** inseparable from **2a_1**; product distribution determined by ^{1}H NMR. [c]After 20 h, a second charge of catalyst (1 mol% $[Ir(cod)OMe]_2$, 3 mol% TrixiePhos) was added, and allowed to react at 170 °C for 20 h. [d]Unable to be fully purified, yield is an upper bound.

With an understanding of the mechanism, we examined the scope of this reaction. The scope with respect to the arene was investigated with mono-, di-, and tri-substituted arenes (**Figure 4**). Electron-rich arenes react well under these conditions (**2aa–2ac**, **2af–2ah**, **2an**, **2ao**), especially compared to electron-poor arenes (**2ad**, **2ae**, **2ai**, **2aj**). Acylation of strongly electron-poor arenes or some functionalized arenes, was not observed. Substitution generally occurs at the most sterically accessible site. When multiple C–H bonds in similar steric environments are available, as in unsymmetrical 1,2-disubstituted arenes **2ah–2aj**, acylation at

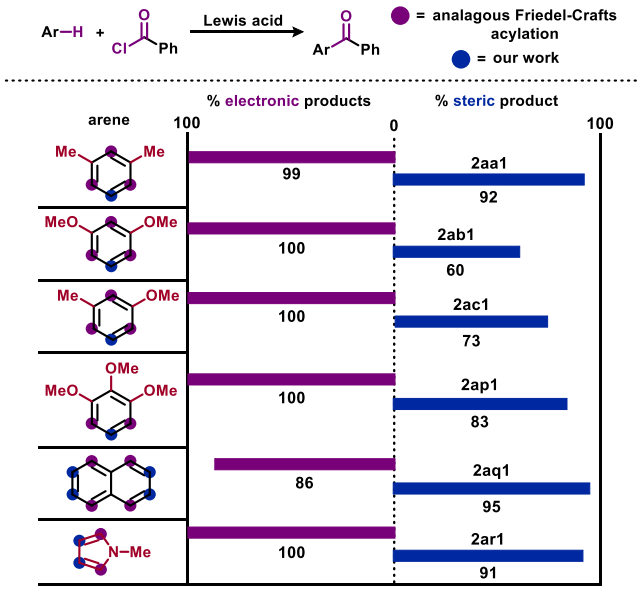

Chart 1. Comparison of Friedel-Crafts acylation electronic-controlled regioselectivity (purple) to our acylation method (blue).

the more electron-rich position is preferred. In the absence of strong electronic effects, mixtures favoring acylation at the more accessible sites result. For example, acylation of toluene (**2am**) provides a 17:17:1 mixture of regioisomers, favoring the *meta* and *para* isomers. As arenes with stronger electron-donors undergo acylation, as in anisole (**2an**) and *N,N*-dimethylaniline (**2ao**), the *para* isomer is favored and the *ortho* isomer is not observed. The reaction tolerates simple arenes with fluoro, trifluoromethyl, methoxy, methyl, methyl ester, and dimethylamino functional groups. *N*-methylated heteroarenes (**2ar**, **2as**) were tolerated, with acylation of *N*-methylpyrrole occurring mostly at the sterically-favored 3-position (10:1 ratio of regioisomers), contrary to Friedel-Crafts acylation.[63] In the case of *N*-methylindole (**2as**), the 3-position relative to the nitrogen is favored both sterically and electronically, thus only one product is observed. Interestingly, naphthalene was acylated almost exclusively at the β-position, the opposite selectivity of Friedel-Crafts acylation.[64] The contrasting regioselectivity of this reaction is summarized in **Chart 1**. The substrates displayed have distinctive electronic/steric-favored sites. Electron rich 1,3-disubstituted arenes show universal selectivity at ortho/para positions with Friedel-Crafts acylation.[46, 63–67] Statistically, the electronically preferred sites for acylation outnumber the sterically accessible sites for many of the arenes in **Chart 1**. Yet, the sterically preferred sites are selectively acylated with our iridium catalyst. Our chemistry shows good selectivity for the steric-controlled product, although with a noticeable decrease in selectivity as the electron density of the ring increases. Very electron poor arenes were not successful with this methodology. In addition, arenes with Lewis basic functional groups (e.g. nitrile, thiophene, carbamates, or acetals) were not successful.

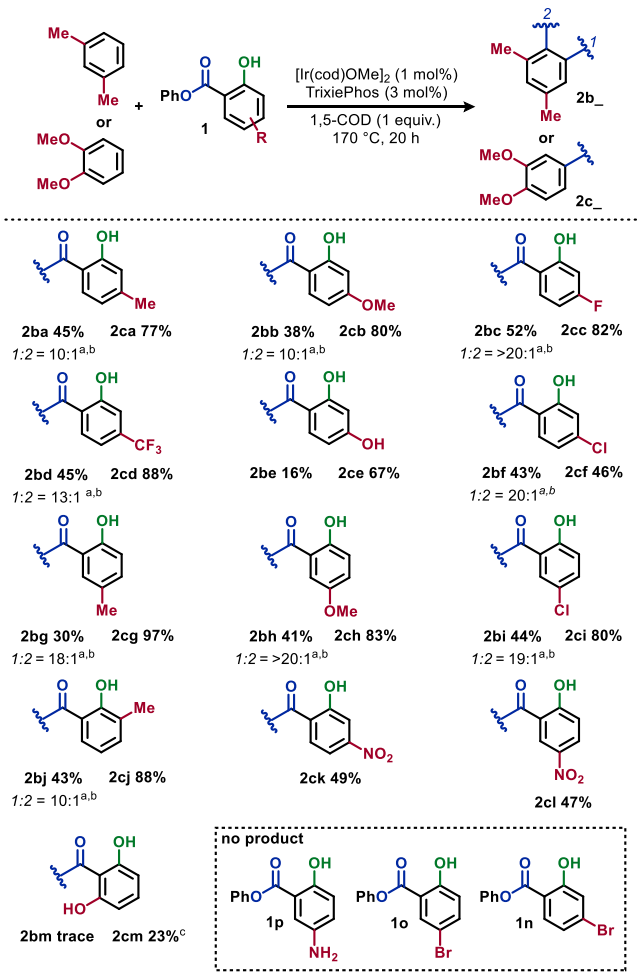

Figure 5. Substrate scope with respect to the salicylate. Performed with phenyl salicylate **1_** (1 equiv), [Ir(cod)OMe]$_2$ (1 mol%), TrixiePhos (3 mol%), 1,5-COD (1 equiv), in arene **1b** or **1c** (0.1 M). For acylation of *m*-xylene (**2b_**), a second charge of catalyst (1 mol% [Ir(cod)OMe]$_2$, 3 mol% TrixiePhos) was added after 20 h, and allowed to react for an additional 20 h. [a]isolated as an inseparable mixture; product distribution determined by ^{1}H NMR. [b]**2b_2** observed and inseparable from mixture; product distribution determined by ^{1}H NMR. [c] Yield determined by ^{1}H NMR; product decomposed during attempted purification.

Next, the scope of arene acylation with respect to the salicylate ester was examined (**Figure 5**). Acylation of *m*-xylene with two charges of catalyst gave the corresponding biaryl ketones in respectable yields. The regioselectivity of the C–H activation still strongly favored the corresponding 1,3,5–substituted products, with at least a >10:1 ratio of isomers. Interestingly, many of the substituted salicylates also yielded **2aa1**, with apparent loss of the functional group R.[68] To access optimal reactivity of these salicylates, acylations were also performed using 1,2-dimethoxybenzene. Due to 1,2-dimethoxybenzene being electron-rich, only one charge of catalyst is required, and only one acylation product was observed under these conditions with no observed loss of

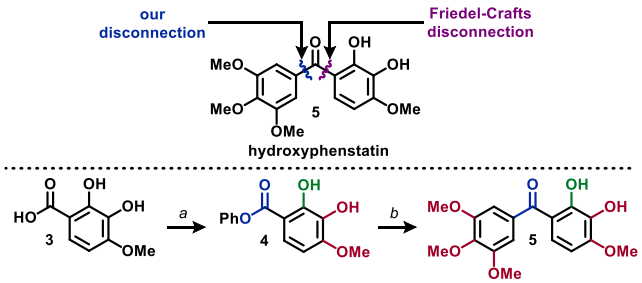

Figure 6. Total synthesis of hydroxyphenstatin **5**. Reagents and conditions: (*a*) $POCl_5$ (1.5 equiv), phenol (20 equiv), 100 °C, 20 hr, 75%. (*b*) $[Ir(cod)OMe]_2$ (3 × 1 mol%), TrixiePhos (3 × 3 mol%), and 1,5-COD (1 equiv) in 1,2,3-trimethoxybenzene (0.1 M), 170 °C, 60 h, 48%. The second and third charges of catalyst were added after 20 and 40 h point.

functional group R. Salicylates with methyl, methoxy, hydroxy, fluoro, and trifluoromethyl substituents all gave products in good yields (67–97%).

Hydroxyl groups were tolerated to varying degrees depending on substitution pattern; product **2ce** was isolated in 67% yield but **2cm** was not isolable due to instability on silica and only observed in 23% yield (quantitative NMR). Likewise, acylation of *m*-xylene yielded a trace amount of potential product (**2bm**), which could not be quantified. Chloro and nitro substituents were similarly tolerated depending on substitution pattern (**2cf**, **2ci**, **2ck**, **2cl**). Phenyl 3-methylsalicylate gave product **2cj** in 88% yield, an intermediate yield relative to the other methyl-substituted salicylates, **2ca** and **2cg**. This implies that steric hindrance around the hydroxyl directing group does not have a strong effect on reactivity. Amino- or bromo-substituted salicylates did not acylate *m*-xylene or 1,2-dimethoxybenzene (**Figure 5**, **1n**–**1p**); for the amino-substituted salicylate **1p** this is likely due to insolubility of the starting material in the reaction conditions.

A noted drawback of this reaction and related C–H borylation/silylation reactions is that a large excess of arene is used, typically in solvent quantities. Under standard conditions, acylation with 78 equivalents of 1,2-dimethoxybenzene yields **2ag** in 93% yield. Acylation reactions using superstoichiometric amounts of 1,2-dimethoxybenzene in mesitylene showed formation of product **2ag**, yielding 30% product with 5 equivalents of arene. Similarly, acylation was observed in 52% yield with 10 equivalents of arene (for additional data, see supplementary information).

With this understanding of the scope of this reaction, we undertook a synthesis of hydroxyphenstatin **4,** a potent anticancer and anti-mitotic target (**Figure 6**).[69] The shortest previous route to synthesize **4** employs a low-yielding, *ortho*- selective Friedel-Crafts acylation of 1,2,3-trihydroxybenzene (25% yield).[70] Our new acylation reaction opens a new disconnection of this target molecule. Di-hydroxy acid **3** can be synthesized in one step from literature procedure.[71] Salicylate ester **4** was synthesized from **3** using phenol and phosphorous oxychloride in 75 % yield. Acylation of 1,2,3-trimethoxybenzene using salicylate ester **4** gave hydroxyphenstatin **5** in 48% yield (36% yield over 2 steps). This synthesis demonstrates a new disconnection available for the synthesis of biologically relevant molecules.

SUMMARY

We have demonstrated the unique mechanistic and synthetic aspects of arene acylation via sequential C–O/C–H activation. Observed KIEs and regioselectivity support that this mechanism is distinct from Friedel-Crafts acylation and offers a pathway to substitution patterns previously inaccessible in a single synthetic step. Steric-controlled acylation is achieved via a proposed concerted metalation deprotonation C–H activation, as supported by experimental and computational evidence. Simple, electron rich arenes are the most successful and a broad range of functional groups are tolerated on the salicylate ester. Steric-controlled acylation was utilized to concisely synthesize an anti-cancer target molecule hydroxyphenstatin. Experimental efforts are underway to study the reverse reaction, change the directing group, lower the temperature and improve reaction yields with stoichiometric quantities of arene. The reaction is a first breakthrough towards forming new C_{acyl}–C_{aryl} bonds under steric control in a single synthetic step using an iridium catalyst.

ASSOCIATED CONTENT

Supporting Information.

Experimental Details for the reaction optimization, initial rates kinetics and kinetic isotope effect data, preparation of new compounds, tabulated characterization data (^{1}H NMR, ^{13}C NMR, melting points, MS, and IR). This material is available free of charge via the internet at http://pubs.acs.org.

AUTHOR INFORMATION

Corresponding Author

*cdouglas@umn.edu

ORCID

Christopher J. Douglas: 0000-0002-1904-6135
Constance A. Anderson: 0000-0002-0321-4640
Nicholas A. Serratore: 0000-0002-2602-425X
Grant B. Frost: 0000-0002-7248-1806
Truong-Giang Hoang: 0000-0003-4368-4142
Steven J. Underwood: 0000-0002-2794-7590

Present Addresses

†Department of Chemistry, National University of Singapore, 3 Science Drive 3, Singapore, 117543.
⊥Department of Chemistry, University of Chicago, 5735 South Ellis Avenue, Chicago, IL, 60637.
§Department of Chemistry, University of California–Berkeley, CA, 94720.

Author Contributions

‡These authors contributed equally.

Notes

The authors declare no competing financial interests.

ACKNOWLEDGMENT

The National Science Foundation (CAREER Award for C.J.D., CHE-1151547) funded this work. C.B.A. thanks the National Science Foundation for a Graduate Research Fellowship (Grant No 00039202). M.A.H. and P.M.G. thank the National Science Foundation for support through the Summer Lando/NSF REU program at the University of Minnesota–Twin Cities (CHE-1359181). We acknowledge the Minnesota Supercomputing Institute (MSI) at the University of Minnesota for providing resources that contributed to the research results reported within this paper. URL: http://www.msi.umn.edu. We thank Dr. Ian Tonks for many helpful discussions. We also thank the reviewers for critically reading and suggesting substantial improvements to an earlier version of this manuscript.

REFERENCES

(1) Johansson Seechurn, C. C. C.; Kitching, M. O.; Colacot, T. J.; Snieckus, V. *Angew. Chem. Int. Ed.* **2012**, *51*, 5062–5085.
(2) He, J.; Wasa, M.; Chan, K. S. L.; Shao, Q.; Yu, J.-Q. *Chem. Rev.* **2017**, *117*, 8754–8786.
(3) Hummel, J. R. ; Boerth, J. A.; Ellman, J. A. *Chem. Rev.* **2017**, 117, 9163–9227.
(4) Kim, D.-S.; Park, W.-J.; Jun C.-H. *Chem. Rev.* **2017**, *117*, 8977–9015.
(5) Newton, C. G.; Wang, S.-G.; Oliveira, C. C.; Cramer, N. *Chem. Rev.* **2017**, *117*, 8908–8976.
(6) Labinger, J. A.; *Chem. Rev.* **2017**, *117*, 8483–8496.
(7) Murakami, K.; Yamada, S.; Kaneda, T.; Itami, K. *Chem. Rev.* **2017**, *117*, 9302–9332.
(8) Leitch, J. A.; Bhonoah, Y.; Frost, C. G. *ACS Catal.* **2017**, *7*, 5618–5627.
(9) Gensch, T.; Hopkinson, M. N.; Glorius, F.; Wencel-Delord J. *Chem. Soc. Rev.* **2016**, *45*, 2900–2936.
(10) Chen, X.; Engle, K. M.; Wang, D.-H.; Yu, J.-Q. *Angew. Chem. Int. Ed.* **2009**, *48*, 5094–5115.
(11) Fumagalli, G.; Stanton, S.; Bower, J. F. *Chem. Rev.* **2017**, *117*, 9404–9432.
(12) Chen, P.-H.; Billett, B. A.; Tsukamoto, T.; Dong, G. *ACS Catal.* **2017**, *7*, 1340–1360.
(13) Souillart, L.; Cramer, N. *Chem. Rev.* **2015**, *115*, 9410–9464.
(14) Chen, F.; Wang, T.;Jiao, N. *Chem. Rev.* **2014**, *114*, 8613–8661.
(15) Takise, R.; Muto, K.; Yamaguchi, J. *Chem. Soc. Rev.***2017**, *46*, 5864–5888.
(16) Dander, J. E.; Garg, N. K. *ACS Catal.* **2017**, *7*, 1413–1423.
(17) Liu, C.; Szostak, M. *Chem. Eur. J.* **2017**, *23*, 7157–7173.
(18) Wang, Q.; Su, Y.; Li, L.; Huang, H. *Chem. Soc. Rev.* **2016**, *45*, 1257–1272.
(19) Ouyang, K.; Hao, W.; Zhang, W.-X.; Xi, Z. *Chem. Rev.* **2015**, *115*, 12045–12090.
(20) Cornella, J.; Zarate, C.; Martin, R. *Chem. Soc. Rev.* **2014**, *43*, 8081–8097.
(21) Wang, R.; Falck, J. R. *RSC Adv.* **2014**, *4*, 1062–1066.
(22) Gooßen, L. J.; Gooßen, K.; Stanciu, C. *Angew. Chem. Int. Ed.* **2009**, *48*, 3569–3571.
(23) Yang, Y.; Lan, J.; You, J. *Chem. Rev.* **2017**, *117*, 8787–8863.
(24) Wei, Y.; Hu, P.; Zhang, M.; Su, W. *Chem. Rev.* **2017**, *117*, 8864–8907.
(25) Nairoukh, Z.; Cormier, M.; Marek I. *Nat. Rev. Chem.* **2017**, *1*, 1–16.
(26) Meng, G.; Szostak, M. *ACS Catal.* **2017**, *7*, 7251–7256.
(27) Meng, G.; Szostak, M. *Org. Lett.* **2016**, *18*, 796–799.
(28) Dong, Z.; Wang, J.; Ren, Z.; Dong, G. *Angew. Chem. Int. Ed.* **2015**, *54*, 12664–12668.
(29) Zhou, P.-X.; Ye, Y.-Y.; Liu, C.; Zhao, L.-B.; Hou, J.-Y.; Chen, D.-Q.; Tang, Q.; Wang, A.-Q.; Zhang, J.-Y.; Huang, Q.-X.; Xu, P.-F.; Liang, Y.-M. *ACS Catal.* **2015**, *5*, 4927–4931.
(30) Mamone, P.; Danoun, G.; Lukas J. Gooßen, L. J. *Angew. Chem. Int. Ed.* **2013**, *52*, 6704–6708.
(31) Hartwig, J. F. *Chem. Soc. Rev.*, **2011**, *40*, 1992–2002.
(32) Press, L. P.; Kosanovich, A. J.; McCulloch, B. J.; Ozerov, O. V. *J. Am. Chem. Soc.* **2016**, *138*, 9487–9497.
(33) Haines, B. E.; Saito, Y.; Segawa, Y.; Itami, K.; Musaev, D. G. *ACS Catal.* **2016**, *6*, 7536–7546.
(34) Dombray, T.; Werncke, C. G.; Jiang, S.; Grellier, M.; Vendier, L.; Bontemps, S.; Sortais, J.-B.; Sabo-Etienne, S.; Darcel, C. *J. Am. Chem. Soc.* **2015**, *137*, 4062–4065.
(35) Cheng, C.; Hartwig, J. F. *J. Am. Chem. Soc.* **2015**, *137*, 592–595.
(36) Cheng, C.; Hartwig, J. F. *Science* **2014**, *343*, 853–857.
(37) Ishiyama, T.; Takagi, J., Hartwig, J. F.; Miyaura, N. *Angew. Chem. Int. Ed.* **2002**, *41*, 3056–3058.
(38) Cho, J. Y.; Tse, M. K.; Holmes, D.; Maleczka, R. E. Jr.; Smith, M. R. III. *Science* **2002**, *295*, 305–308.
(39) Brown, A. C.; Gibson, J. *J. Chem. Soc., Trans.* **1892**, *61*, 367–369.
(40) Wu, X.-F. *Chem. Eur.J* **2015**, *21*, 12252–12265.
(41) Huang, Y.; Zhu R.; Zhao, K.; Gu, Z. *Angew.Chem. Int. Ed.* **2015**, *54*, 12669–12672.
(42) Akai S., Peat, A. J.; Buchwald, S. L. *J. Am. Chem. Soc.* **1998**, *120*, 9119–9125.
(43) Gautam, P.; Bhanage, B. M. *J. Org. Chem.* **2015**, *80*, 7810–7815
(44) Lin, X.-F.; Li, Y.; Li, S.-Y.; Xiao, Z.-K.; Lu, J.-M. *Tetrahedron* **2012**, *68*, 5806–5809.
(45) Hoang, G. T.; Pan, Z.; Brethorst, J. T.; Douglas, C. J. *J. Org. Chem.* **2014**, *79*, 11383–11394.
(46) *m*-xylene Friedel-Crafts regioselectivity with benzoyl chloride: Kusama, H.; Narasaka, K. *Bull. Chem. Soc. Jpn*. **1995**, *68*, 2379–2383.
(47) The configuration of oxidative addition intermediate **III** was proposed after comparison with **III²** (See **Figure 3**)
(48) The configuration of TrixiePhos complex **V** was proposed after comparison with JohnPhos angalogues $\mathbf{V_{JP}^{1\text{-}3}}$ (See **Figure 3**)
(49) Lapointe, D.; Fagnou, K. *Chem. Lett.* **2010**, *39*, 1118–1126.
(50) Davies, D. L.; Macgregor, S. A.; McMullin, C. L. *Chem. Rev.* **2017**, *117*, 8649–8709.
(51) Experiments and analysis were performed as detailed in: Simmons, E. M.; Hartwig J. F. *Angew. Chem. Int. Ed.* **2012**, *51*, 3066–3072. (and references within)
(52) For simplification of discussion our KIE data analysis is presented in context of the phenoxide-assisted 4-member CMD transition state. A carboxylate-assisted 6-member CMD transition state would also be consistent with the data.
(53) Sibbald, P. A., Rosewall, C. F., Swartz, R. D., Michael, F. E. *J. Am. Chem. Soc.* **2009**, *131*, 15945–15951.
(54) Churchill, D. G.; Janak, K. E.; Wittenberg, J. S.; Parkin, G. *J. Am. Chem. Soc.* **2003**, *125*, 1403–1420.
(55) Song, Z.; Beak, P. *J. Am. Chem. Soc.* **1990**, *112*, 8126–8134.
(56) Adam, W.; Krebs, O.; Orfanopoulos, M.; Stratakis, M.; Vougioukalakis, G. C. *J. Org. Chem.* **2003**, *68*, 2420–2425.
(57) Jones, W. D. *Acc. Chem. Res.* **2003**, *36*, 140-146.
(58) Boller, T. M.; Murphy, J. M.; Hapke, M.; Ishiyama, T.; Miyaura, N.; Hartwig, J. F. *J. Am. Chem. Soc.* **2005**, *127*, 14263–14278.
(59) Zhu, H.; Meyer, M. P. *Chem. Commun.* **2011**, *47*, 409–411.
(60) Vaska, L.; DiLuzio J. W. *J. Am. Chem. Soc.* **1961**, *83*, 2784–2785.
(61) Yu, H. S.; He, X.; Truhlar, D. G. *J. Chem. Theory Comput.* **2016**. *12*, 1280–1293.
(62) M06 and M06-L computations are found in the supporting information

(63) *N*-methylpyrrole Friedel-Crafts regioselectivity with benzoyl chloride: He, F.; Wu, H.; Chen, J.; Su, W. *Synth. Commun.* **2008**, *38*, 255–264.
(64) Naphthalene Friedel-Crafts regioselectivity with benzoyl chloride: Earle M. J.; Hakala, U.; Hardacre, C.; Karkkainen, J.; McAuley, B. J.; Rooney, D. W.; Seddon, K. R.; Thompson, J. M.; Wähälä, K. *Chem. Commun.* **2005**, *7*, 903–905.
(65) 1,3-Dimethoxybenzene Friedel-Crafts regioselectivity with benzoyl chloride: Vekariya, R. H.; Aubé J. *Org. Lett.* **2016**, *18*, 3534–3537.
(66) 3-Methylanisole Friedel-Crafts regioselectivity with benzoyl chloride: Miquel, J. F.; Buu-Hoi, N. G.; Royer, R. *J. Chem. Soc.* **1955**, 3417–3419
(67) 1,2,3-Trimethoxybenzene Friedel-Crafts regioselectivity with benzoyl chloride: Sato, H.; Dan, T.; Onuma, E.; Tanaka, H.; Aoki, B.; Koga, H. *Chem. Pharm. Bull.* **1992**, *40*, 109–116.
(68) Experiments to study this apparent defunctionalization are underway.
(69) Pettit, G. R.; Grealish, M. P.; Herald, D. L.; Boyd, M. R.; Hamel, E. Pettit, R. K. *J. Med. Chem.* **2000**, *43*, 2731–2737.
(70) Radha, P. *Synth. Commun.* **2003**, *33*, 3869–3873.
(71) Yanagisawa, A.; Taga, M.; Atsumi, T.; Nishimura, K.; Ando, K.; Taguchi, T.; Tsumuki, H.; Chujo, I.; Mohri, S. *Org. Process Res. Dev.* **2011**, *15*, 376–381.

Graphical Abstract